Applied Materials Today xxx (xxxx) xxx

Contents lists available at ScienceDirect

Applied Materials Today

journal homepage: www.elsevier.com/locate/apmt

Metallic glass based composites with precise tunable thermal expansion

Fei Sun, Hongji Lin, Jianan Fu, Zhen Li, Feng Luo, Bei Wang, Wenqing Ruan, Shuai Ren, Zhenxuan Zhang, Xiong Liang, Jiang Ma *, Jun Shen

Shenzhen Key Laboratory of High Performance Nontraditional Manufacturing, College of Mechatronics and Control Engineering, Shenzhen University, Shenzhen 518060, China

ARTICLE INFO

Keywords:
Metallic-glasses based composites
Tunable thermal expansion
Continuous and precise regulation
Near-zero thermal expansion

ABSTRACT

Thermal expansion properties of materials are of fundamental interest and regulation of thermal expansion is significant for practical applications, but remains a challenge. We developed a moderate and efficient route for the preparation of metallic glass matrix composites, enabling precise tuning of thermal expansion properties over a wide range. Admixtures with dissimilar thermal expansion properties were successfully bonded to metallic glasses because of the unique thermoplasticity. The prepared composites achieve continuous regulation of the coefficient of thermal expansion over a broad range (9.6 ppm/K to 34 ppm/K), and high precision (0.065 ppm/K corresponds to one percent of the volume) can be realized. In addition, composites with nearly zero thermal expansion properties (average 0.19 ppm/K) in the wide temperature region (223 K to 473 K) were successfully prepared. Our approach provides a flexible and moderate pathway to achieve precise customization thermal expansion properties, promising a shift from laborious searching to precise tailoring of materials.

1. Introduction

Most solid materials exhibit positive expansion with increasing temperature, only a few exhibits negative or zero expansion [1–4]. In practical engineering applications, improper thermal expansion always leads to premature failure of components, thus thermal expansion properties of materials are required to match different application scenarios. Materials that can match ambient temperatures and exhibit targeted dimensional variations hold significant promise for applications in sensors, pipe connections, and dental fillings [5–7]. In the fields of precision instruments and optical communication systems, components are required to maintain dimensional stability under temperature changes to ensure the accuracy and extend the service life of the instruments [8,9]. Materials that capable of achieving targeted area/-volume changes in response to temperature variations are urgently needed. However, the thermal expansion properties are determined by the intrinsic structure of the material, it is difficult to meet the complex application environment simply by the materials selection.

The ability to accurately tailor the coefficient of thermal expansion (CTE) properties of materials is desirable for the complex practical engineering applications. To address this challenge, the preparation of composites by combining materials with different thermal expansion properties for the regulation of CTE is considered as a feasible way [10–13]. Based on this strategy, negative thermal expansion (NTE) materials (e.g., zirconium tungstate, beta-eucryptite) are selected as expansion inhibitors and sintered with reinforcing materials (e.g., Cu, Al) to prepare composites with required thermal expansion properties [14–22]. However, in the past works, more attention has been focused on the preparation of nearly zero thermal expansion (NZTE) materials, while fine tuning of thermal expansion properties over a wide range has rarely been reported. In addition, NTE materials are usually metastable and tend to decompose when the temperature is slightly higher [23]. While the soften temperature of these reinforcing materials is generally very high, and the sintering process is always time-consuming, which will cause severe interfacial reactions and increase the risk of failure of the expansion inhibitor [23,24]. Metallic glasses (MGs), which was first discovered in 1960, combine the excellent properties of metals and glasses [25]. Unlike conventional metals that need to be heated to the high melting temperature, MG has excellent fluidity in a temperature span called supercooled liquid region (SLR) [26–30]. It means that MG can be bonded together with other materials at a mild temperature. Our recent work has demonstrated that La-based MG can be used as "metallic glue" to bond various materials into compact and designable composites when the temperature is slightly above the glass transition temperature (T_g, about 460 K) [11]. In addition, MGs exhibit a lower CTE and excellent mechanical properties [31–33], as a result, MGs can

* Corresponding author.
E-mail address: majiang@szu.edu.cn (J. Ma).

https://doi.org/10.1016/j.apmt.2022.101565
Received 10 April 2022; Received in revised form 12 June 2022; Accepted 15 June 2022
2352-9407/© 2022 Elsevier Ltd. All rights reserved.

significantly broaden the range of CTE that can be regulated and greatly improve the mechanical properties of composites.

This paper develops a moderate and efficient route to realize the precisely design and continuous adjustment of the thermal expansion properties. To modulate the CTE in a wide range as well as to verify the accuracy of the modulation, La-based MG particles were used as the reinforcing phase and binder to be compounded with pure zinc (Zn), high entropy alloy (HEA), and beta-eucryptite, respectively. The low preparation temperatures (~480 K, slightly above the T_g of La-based MG) and short pressurization time (less than 3 min) during the whole fabrication process minimize interfacial reactions and ensure the stability of the NTE materials. Precise regulation (0.065 ppm/K corresponds to one percent of the volume) of the CTE of the composite material over a very wide range (9.6 ppm/K to 34 ppm/K) can be achieved by adjusting the addition ratio of MG and admixtures. In particular, by adjusting the addition ratio of beta-LAS, we achieved MG-beta-LAS composites with nearly zero thermal expansion (NZTE) characteristic over a wide temperature range (223 K to 473 K), which has great potential for applications in precision instruments, aerospace and other fields. Our results provide an excellent strategy for precise customization of CTE over a wide range, promising a shift from laborious searching to precise tailoring of materials, which will greatly satisfy applications in temperature-sensitive function materials and devices.

2. Materials and experimental

2.1. Fabrication the composites

In order to obtain composites with predetermined thermal expansion properties, MG particles and admixtures (Zn, HEA, beta-LAS) with dissimilar CTE Performance were mixed uniformly at the designed volume fraction and placed into the mold cavity. Then the system was evacuated and a pre-pressure of 1 kN was applied to mixtures. When the system temperature was heated to the SLR of La-based MG (~480K), a strain rate of 0.05 mm/s of 5 kN pressure was applied and maintained for 1 min. Under the action of pressure, the mixture formed a dense solid due to the excellent mobility of MG, and then was rapidly cooled.

2.2. Materials preparation

The La-based MG $La_{55}Al_{25}Ni_5Cu_{10}Co_5$ (at.%) was chosen for the present work because of its wide SLR and excellent mobility at moderate temperatures. The MG ribbons were prepared by a conventional melt spinning process. Subsequently, MG ribbons were cut into small particles with an average particle size of approximately 150 μm. To realize a larger adjustable range of CTE, Zn powders with positive CTE (34 ppm/K) and beta-LAS powders with negative CTE (-6.1 ppm/K) were purchased directly from commercial suppliers. To verify the accuracy of the regulation of the thermal expansion properties, we additionally purchased HEA ($Co_{20}Cr_{20}Fe_{20}Ni_{20}Mn_{20}$) powders with a CTE (16 ppm/K) close to La-based MG (9.6 ppm/K). The average particle size of the above three admixtures is about 10 μm. Subsequently, the MG particles were mixed evenly with the admixtures by repeated stirring and shaking, respectively.

2.3. Multi-scale structural characterizations

X-ray diffraction (XRD; Rigaku MiniFlex600) with Cu Kα radiation was used to identify MG particles and admixtures as well as the final composite obtained. Differential scanning calorimetry (DSC; Perkin–Elmer DSC-8000) at a heating rate of 20 K/min was used to detect La-based MG particles. The micro morphology and elemental distribution of composites were characterized using a field emission scanning electron microscope (SEM; FEI QUANTA FEG 450) instrument. The atomic structure was characterized using a transmission electron microscopy (TEM; JEM-2100F) with EDS. The TEM samples were prepared on a FEI Scios SEM/FIB dual beam system. A High-resolution computed tomography system (CT, Sanying precision instruments-nano Voxel 3000d, China) was used to detect possible defects within the composite material. CTE measurements were conducted using a thermal mechanical analyzer (TMA;402 F3, NETZSCH, Germany) at a heating rate of 5 K/min under a N_2 atmosphere. The temperature measurement range is about 120~1800 K, the displacement resolution is 0.125 nm, and the load resolution is less than 0.01 mN. All samples prepared for testing the CTE were cylinders of 5 mm in diameter and 10 mm in length. Compression test of composites was conducted on Zwick electronic universal testing machine (Z050 TEW, strain rate 0.001 s^{-1}). All samples prepared for the compression test were cylinder with a length/diameter ratio of 1.5 (length 7.5 mm and diameter 5 mm), which is conformity with ASTM standard [34]. Prior to the compression and thermal expansion tests, the ends of the samples were polished to be parallel to each other.

3. Results and discussion

3.1. Bonding mechanism

Fig. 1a graphically depicts the preparation process of the composite, and through this process MG with various admixtures can be prepared into dense and homogeneous blocks. The bonding state largely determines the mechanical properties of the composites, it is necessary to investigate the bonding mechanism of MG with admixtures. Here, the composites prepared by MG and Zn were selected to investigate the bonding mechanism. Fig. 1(b, c) show the SEM images of MG and Zn particles. The T_g and crystallization temperature (T_x) of La-based MG were measured to be 460 K, 514 K respectively by DSC (see Fig. S1). The photograph of the composite prepared with MG and Zn particles in equal volume fractions is shown in Fig. 1d. It can be seen that MG-Zn composite is a dense solid. Fig. 1e shows the fracture surface morphology of the MG-Zn composite observed by SEM. It can be clearly found that the flow of MG fills the voids between the Zn powders and binds the Zn particles tightly together like a glue, which indicates that the MG-Zn composite is dense and integrity. To investigate the distribution of MG and Zn within the composite and the bonding quality at the interface, the morphology of polished MG-Zn composite was observed at different magnifications using the backscattering mode, the results are presented in Fig. 1(f, g). We can find that the MG (bright phase) and Zn (dark phase) are uniformly distributed, and Zn is tightly wrapped by the flowing MG, which further confirms the dense nature of the composite. To further understand the bonding mechanism of the composite, TEM was applied to characterize the interface between MG and Zn. The detail of the interface is shown in Fig. 1g and no cracks can be observed, which proves the perfect combination between MG and Zn. Fig. 1(h–j) show the high-resolution structures at the combination area (Zn region, interface region, and MG region, respectively) observed by high-resolution transmission electron microscopy (HRTEM). It can be clearly observed that the three regions show different atomic structures, the Zn region is a typical crystalline structure, the MG region is a typical amorphous structure, and the interface region is a combination of ordered and disordered structures. Accordingly, three regions R1, R2, and R3 marked in the HRTEM images were chosen for selected area electron diffraction (SAED), the results are shown in Fig. 1(k–m), respectively. The diffraction pattern in the R1 region shows a typical crystalline state, which corresponds to Zn. The R2 region at the interface shows a combination of crystal spots and a halo ring. Furthermore, the R3 region corresponding to MG shows a pure diffraction ring, which indicates that the amorphous nature of MG is maintained. We also use the EDS to analyze the distribution of elements at the composite interface and the results are presented in Fig. 1n. It can be found that the distribution of elements in the MG region and Zn region at the interface is not entirely distinct, obviously, a part of the elements belonging to MG diffused towards the Zn-rich region. The above results reveal that MG and Zn are

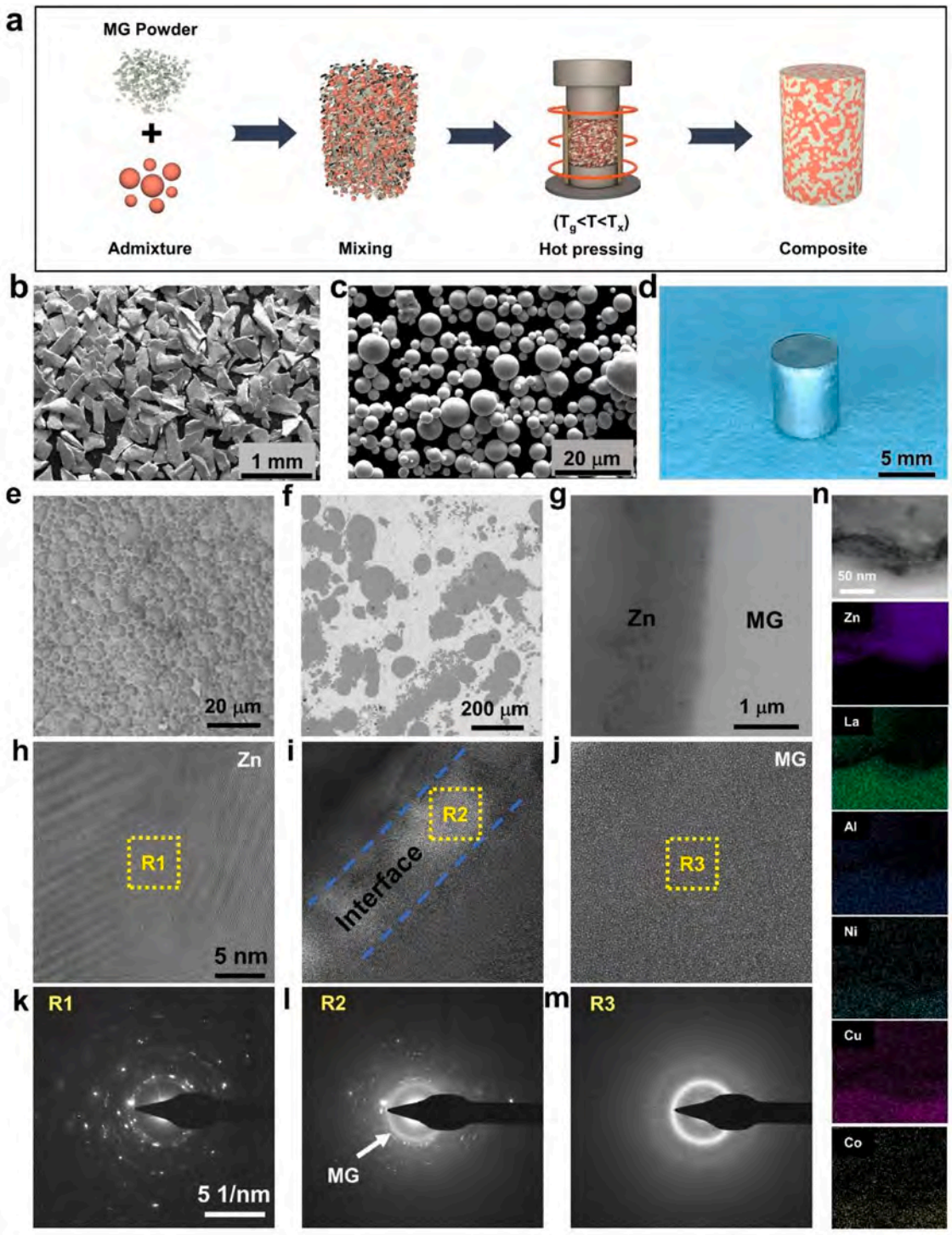

Fig. 1. Schematic diagram of composite preparation and characterization of binding quality. (a) Schematic diagram of the preparation process of composite materials. (b) SEM image of MG particles. (c) SEM image of Zn powders. (d) Photograph of MG-Zn composite. (e) Fracture surface morphology of MG-Zn composites. (f-g) SEM morphology of the polished MG-Zn composite at different magnifications. (h-j) High-resolution TEM images of the composite in Zn region, interface region and MG region. (k-m) Diffraction patterns of the regions R1, R2 and R3. (n) Elemental distribution of the composite at the interface.

not simply mechanically combined, but completely connected as a whole by breaking through the surface oxide layer, which will bring a synergy effect of their mechanical and thermal properties.

3.2. Regulation of CTE in wide range

In order to achieve the regulation of expansion properties over a wide range, Zn, which has the greatest CTE (34 ppm/K) among conventional solid materials [35], was selected as an admixture to bond with MG. The expansion properties of pure Zn, pure MG, and MG-Zn composites in the temperature range of 310-430 K are presented in Fig. 2a. The volume fractions of Zn in the composites are 90, 70, 50, 30, and 10 vol%, respectively. The linear CTE of a material is defined as:

$$\alpha = \frac{\Delta L}{L_0 \Delta T} \tag{1}$$

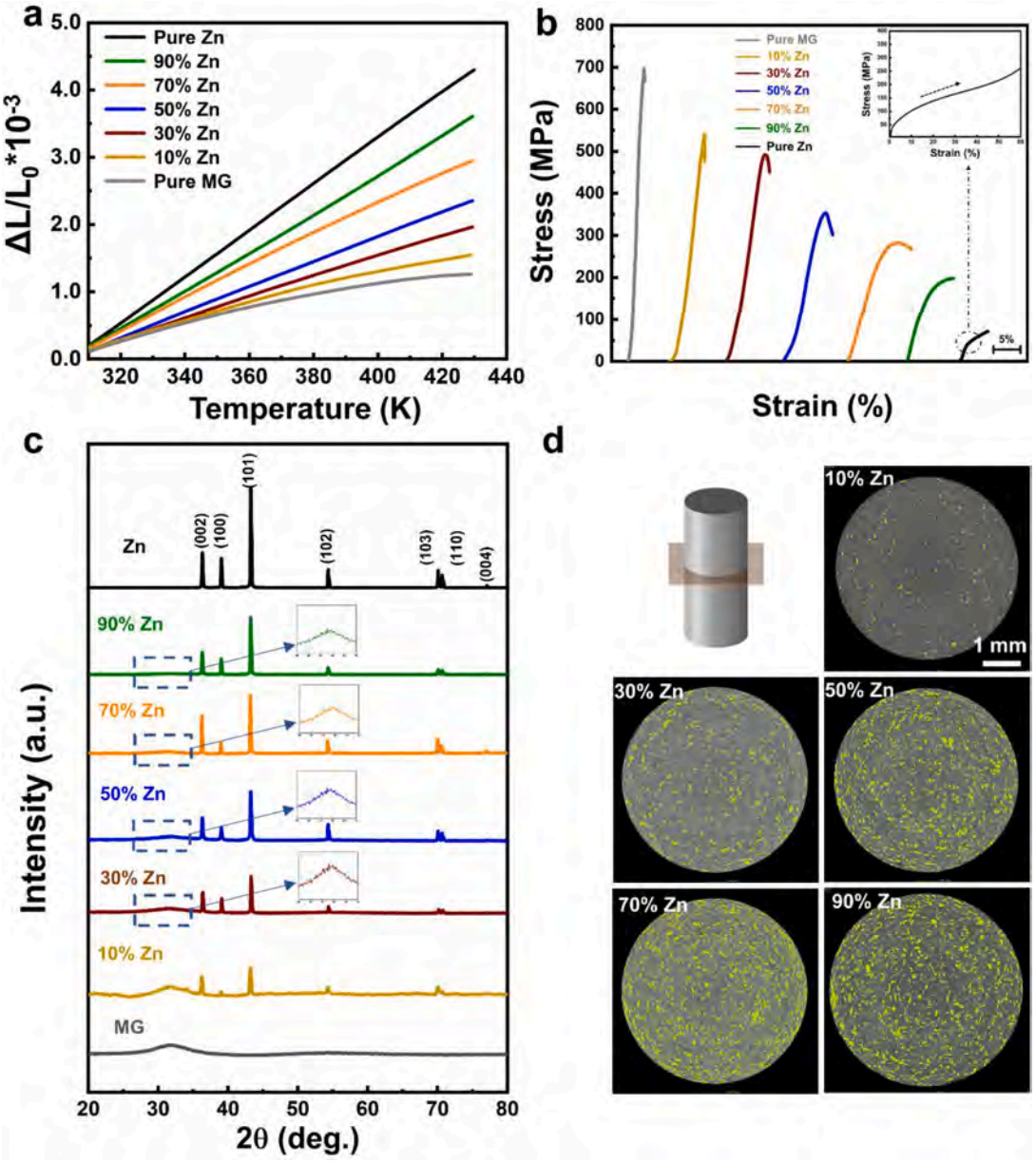

Fig. 2. Performance and structural characterization of MG-Zn composites. (a) Expansion properties of MG-Zn composites with Zn volume ratio from 0 to 100 vol%. (b) Compressive properties of MG-Zn composites with different Zn ratios. (c) XRD patterns of MG-Zn composites with Zn volume ratios from 0 to 100 vol%. (d) The high-resolution CT images corresponding to MG-Zn composites with Zn volume ratios from 10 to 90 vol%.

In Eq. (1), ΔL denotes the elongation of the sample length, L_0 represents the original length of the sample, and ΔT is the corresponding change in temperature. According to Eq. (1), the linear CTEs of Zn and MG can be calculated to be 34 ppm/K and 9.6 ppm/K, respectively. The corresponding CTEs of MG-Zn composites were 28.4 ppm/K, 23.3 ppm/K, 18.6 ppm/K, 15.3 ppm/K, and 11.9 ppm/K, respectively. It can be found that as the addition ratio of Zn decreases, the CTE of the composite material also gradually decreases proportionally. The theoretical CTE value of composite α_T can be given in the form of Turner's law [36]:

$$\alpha_T = \frac{\frac{\alpha_1 P_1 K_1}{d_1} + \frac{\alpha_2 P_2 K_2}{d_2} + \ldots + \frac{\alpha_n P_n K_n}{d_n}}{\frac{P_1 K_1}{d_1} + \frac{P_2 K_2}{d_2} + \ldots + \frac{P_n K_n}{d_n}} \quad (2)$$

In Eq. (2), α_n represents the CTE of the corresponding group element, P_n represents the mass fraction of each component, K_n is the bulk modulus of each component, and d_n means the density of each component. The mass fraction P_n can be obtained by simple calculation of density d_n and volume ratio.In the present work, the linear CTE for MG and Zn is 34 ppm/K and 9.6 ppm/K, respectively. Based on Eq. (2), we can calculate that when the volume fraction of Zn is 90, 70, 50, 30, 10 vol%, the theoretical linear CTE of the corresponding composites is 32.4 ppm/K, 28.7 ppm/K, 24.5 ppm/K, 19.4 ppm/K, 13.2 ppm/K, respectively. To facilitate comparison, we plotted the theoretical and experimental values of MG-Zn composites with different addition ratios of Zn (see Fig. S2). It can be found that the experimental and theoretical values of the composite CTE are close to each other, indicating that it is highly feasible to tailor the target CTE by adjusting the ratio of the admixture. Using this strategy, we achieved a gradient adjustment of the material expansion coefficient from 9.6 ppm/K (pure MG) to 34 ppm/K (pure Zn). In addition, the compressive properties of MG-Zn composites with different Zn ratios were tested. As presented in Fig. 2b, the La-based MG shows a large compressive strength of 714 MPa, but a poor plasticity. Although the yield strength of the Zn is only 50 MPa, it shows excellent compression plasticity. The composites have the advantages of

MG and Zn, and the strength and plasticity of the composites show a clear tendency with the variation of the ratios. This means that the composites match different application scenarios with the most appropriate mechanical properties, and thermal expansion properties can be customized. Fig. 2c shows the XRD patterns of the composites with Zn percentages of 90, 70, 50, 30, and 10 vol%, the XRD patterns of pure MG and pure Zn are also included. It can be seen that the XRD pattern of Zn is a characteristic crystalline peak while the MG is a broad amorphous peak. The XRD patterns of the composites are a combination of two types of peaks, and show a trend of gradually increasing amorphous peaks and decreasing crystalline peaks as the Zn content decreases. The XRD results reveal the internal structure of the MG-Zn composites, which are consistent with the previous TEM results. To evaluate the internal homogeneity and densities of composite materials, high-resolution CT scans were used to examine samples. Fig. 2d presents the scanning results of the cross section at the middle of the samples, and the scanning results of other height sections are shown in Fig. S3. It can be found that the distribution of MG (gray phase) and Zn (fluorescent phase) in the composite material is uniform, and no obvious cracks can be seen. Furthermore, Archimedes' principle was used to detect the actual density of MG, Zn and composites. The actual density ρ_{actual} of the sample can be expressed as:

$$\rho_{actual} = (\omega_1 \times \rho_1)/(\omega_1 - \omega_2) \quad (3)$$

In Eq. (3), ρ_1 denotes the density of distilled water (0.999 g/cm^3) at room temperature, ω_1, ω_2 represent the weight of the measured object in air and distilled water, respectively. Here, the measured actual densities of MG and Zn were 5.819 g/cm^3, 7.149 g/cm^3, respectively. The corresponding theoretical density $\rho_{theoretical}$ of the composites can be given as:

$$\rho_{theoretical} = \sum_{i=1}^{n} v_i \rho_i \quad (4)$$

Where v_i, ρ_i, represent the volume fraction and density of each admixture in the composite, respectively. According to Eqs. (1) and (2), the calculated actual and theoretical densities of the composites were plotted in Fig. S4. It is clear that the actual density of the composites is very close to the theoretical density, and the smallest relative density is greater than 96.5%. These results indicate that the use of MG as a bonding agent is an excellent strategy for preparing dense solids and regulating material properties.

3.3. Precise regulation of CTE

To verify the accuracy of the regulation of thermal expansion properties, HEA was chosen to be combined with La-based MG to prepare composites. The CTE of HEA selected in this work is 16 ppm/K [10], which is close to the CTE of La-based MG. Fig. 3a shows the SEM image of HEA powders, the average particle size is about 10 μm. To tailor the thermal expansion properties within such a narrow range, composites containing 10, 30, 50, 70, and 90 vol% of HEA were prepared, respectively. Fig. 3b presents the MG-HEA composite prepared with MG and HEA in equal volume fractions, we can find that the sample is dense and homogeneous. The intrinsic structure of MG-HEA composites as well as MG and HEA were characterized by XRD and is displayed in Fig. 3c. It can be clearly found that the XRD patterns of the composites are a combination of amorphous peaks and crystalline peaks of HEA. The intensity of the crystalline peaks decreases with the reduction of HEA addition and the intensity of the corresponding amorphous peaks

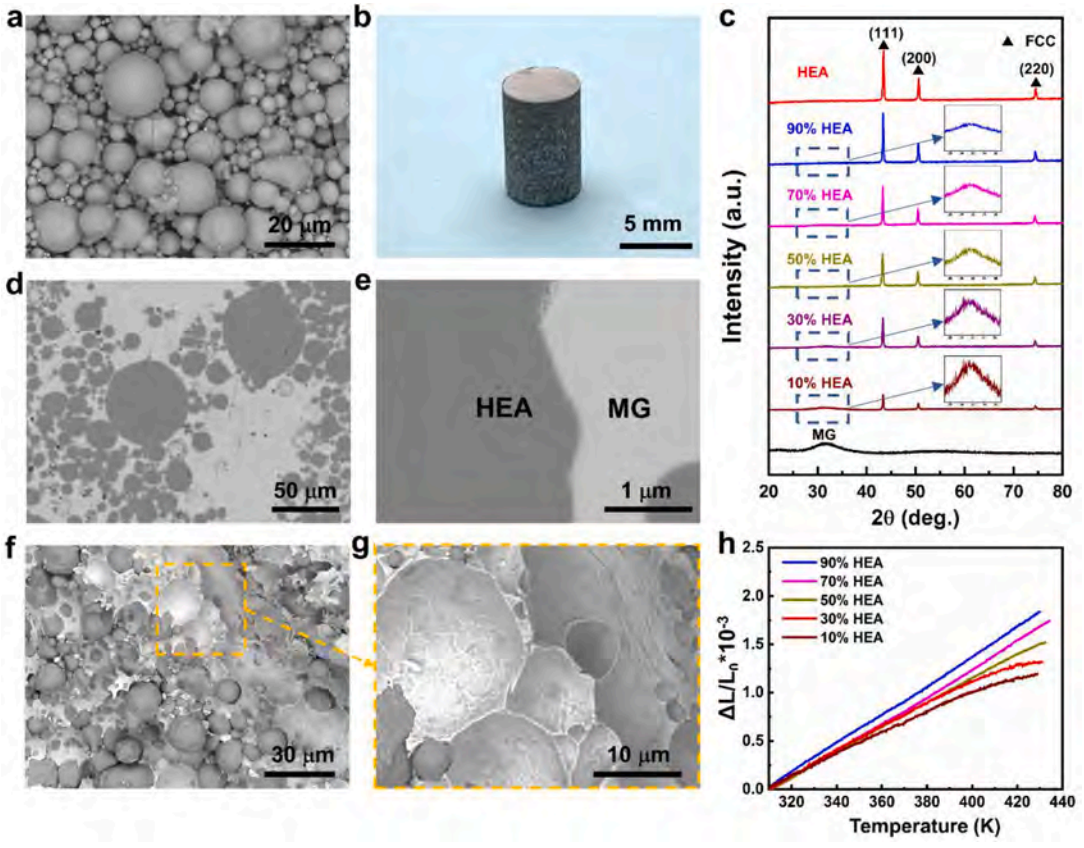

Fig. 3. Performance and structural characterization of MG-HEA composites. (a) SEM image of HEA particles. (b) Photograph of composite prepared with MG and HEA. (c) XRD patterns of MG-HEA composites with HEA volume ratios from 0 to 100 vol%. (d, e) SEM morphology of the MG-HEA composite interface at different magnifications. (f, g) Fracture surface morphology of MG-HEA composite at different magnifications. (h) Expansion properties of MG-HEA composites with HEA volume ratio from 10 to 90 vol%.

increases. The bonding quality of MG-HEA composites was deeply explored by SEM observation. As shown in Fig. 3d, the backscattered images of the polished sample illustrate the distribution of MG and HEA. Clearly, significant flow of MG (bright phase) occurred during hot pressing to encapsulate the HEA particles (dark phase). Fig. 3e shows a high magnification image of the binding of MG and HEA at the interface, and it can be found that the binding of the two phases is tight and reliable. Correspondingly, the fracture morphology of the composite was observed. As shown in Fig. 3f and its enlarged image (see Fig. 3g), MG binds to HEA like a glue, which is consistent with the results in Fig. 3d. The above SEM results reveal the bonding mechanism of MG and HEA, further proving the denseness and reliable quality of the composite. Fig. 3h shows the expansion properties of MG-HEA composites with different HEA contents in the range of 310−430 K. The linear CTE of MG-HEA composites with 90, 70, 50, 30, 10 vol% of HEA is 15.1 ppm/K, 13.9 ppm/K, 12.4 ppm/K, 11.0 ppm/K, 9.7 ppm/K, respectively. The experimental values and corresponding theoretical values (calculated according to the Eq. (2)) of MG-HEA composites with different HEA ratios are shown in Fig. S5. It can be found that the experimental value of CTE is very close to the theoretical one, and approximately 0.065 ppm/K corresponds to a change of one percent of the volume. It means that in such a narrow range of CTE, the thermal expansion properties of the composites can also be precisely tailored by continuously adjusting the proportion of the admixture.

3.4. Nearly zero expansion composites

Following the above strategy, we can also successfully conduct the preparation of composites with NZTE properties. The typical NTE material beta-LAS with an average thermal expansion coefficient of -6.1 ppm/K was used as expansion inhibitor to compound with MG. The average particle size of the beta-LAS powders is about 10 μm, and its SEM image is displayed in Fig. 4a. A photograph of the composite fabricated from beta-LAS and MG in equal volume fractions is shown in Fig. 4b, it can be seen that the ceramic particles are successfully bonded tightly by the MG glue at low temperatures. The volume fractions of 30, 45, and 60 vol% of beta-LAS were added to prepare MG-beta-LAS composites, respectively. The corresponding thermal expansion properties are shown in Fig. 4c, we can find that the CTE of the composites decreases significantly with the increase of beta-LAS addition ratio. In particular, the composite exhibited NZTE performance (0.19 ppm/K) over a broad temperature range (220−480 K) when beta-LAS was added at 60 vol%. High-resolution CT was used to characterize the interior of the corresponding zero-expansion MG-beta-LAS composite, the results are shown in Figs. 4d and S3. It can be clearly seen that the distribution of MG and beta-LAS is homogeneous and consistent. Correspondingly, to explore the bonding quality inside the material, the fracture surface morphology of the zero-expansion composite was probed using the backscattering mode. As shown in Fig. 4(e, f), the excellent fluidity within the SLR enables the MG to adequately fill the interstices between the ceramic particles, which contributes to the formation of dense solids. Mechanical property is one of the key concerns for engineering applications, the compression property of zero expansion composite was tested. As shown in Fig. 4g, the NZTE composite exhibits excellent mechanical properties due to the MG reinforcement. The compressive strength is 250 MPa, with about 6% compressive plasticity, showing great prospects for engineering applications. The XRD result (see Fig. 4h) reveals the internal structure of the composite as a combination

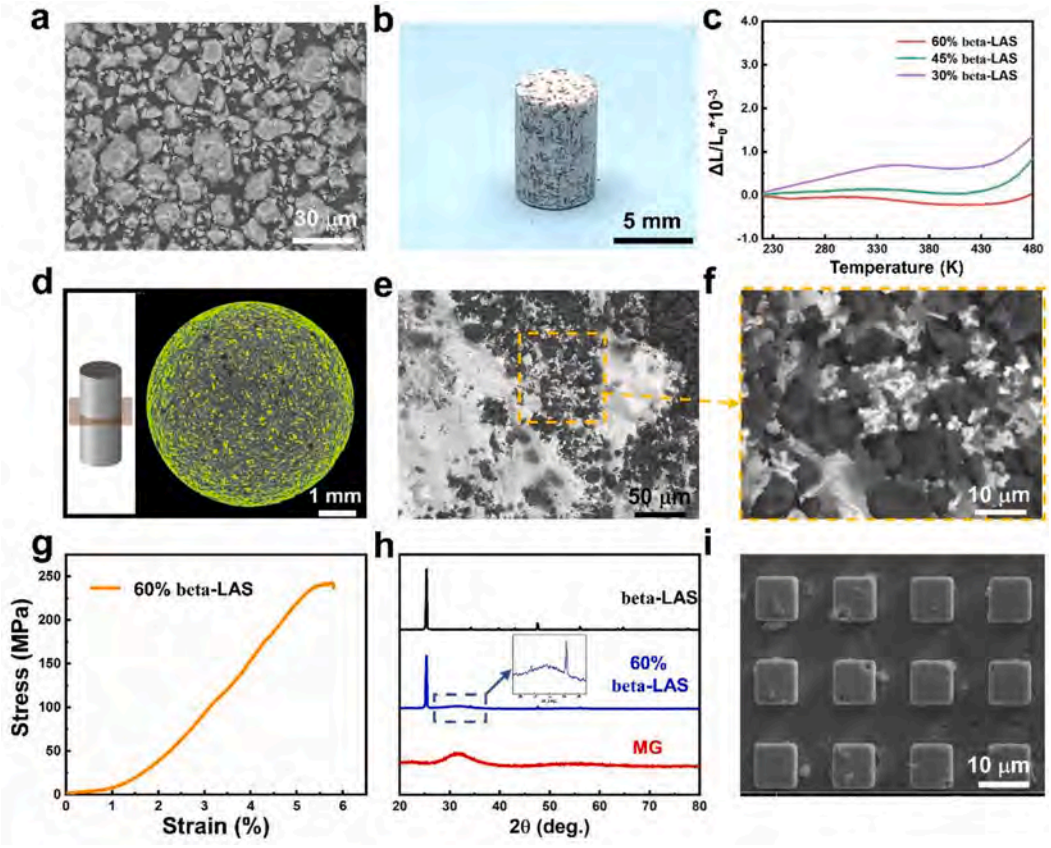

Fig. 4. Performance and structural characterization of MG-beta-LAS composites. (a) SEM image of beta-LAS powders. (b) Photograph of composite prepared with MG and beta-LAS. (c) Expansion properties of MG-beta-LAS composites with beta-LAS volume ratio from 30 to 60 vol%. (d) The high-resolution CT image of MG-beta-LAS composite with 60 vol% beta-LAS. (e, f) Fracture surface morphology of MG-beta-LAS composite at different magnifications. (g) Mechanical properties of MG-beta-LAS composites with 60 vol% beta-LAS. (h) The XRD patterns of MG, beta-LAS and composite containing 60 vol% beta-LAS. (i) Microstructures fabricated by NZTE composites.

of the amorphous peak of MG and the crystalline peak of beta-LAS, which is consistent with the previous results. In addition, the fluidity of MG in SLR endows the composite with good processability. When the temperature rises to the SLR, the beta-LAS particles inside the composite flow with the softening MG under the action of pressure. This means that structures with zero expansion characteristics can be easily manufactured by hot embossing, the shape of which depends on the design of the concave die. As an example, Fig. 4i shows the array microstructure obtained by secondary thermal imprinting. This indicates that NTZE composites prepared based on MG also have convenient processability and show great potential for applications in precision instruments, aerospace, etc. Fig. 5(a–c) summarize the processing parameters (time, temperature) and NZTE temperature range of MG-beta-LAS composites with other NZTE materials in references (Table S1). It is clearly that most NZTE materials need to be prepared at very high temperatures for a long time, while the MG-beta-LAS composites fabricated in this work with NZTE performance (average 0.19 ppm/K) over a broad temperature range (220-480 K) can be prepared immediately at mild temperatures. The proposed efficient and moderate pathway will significantly reduce the cost of NZTE materials and improve the reliability of the composites.

4. Conclusion

In summary, this work developed a moderate and convenient strategy to prepare metallic glass matrix composites with continuously and precisely tunable CTE. Benefiting from the excellent mobility of MG within the SLR, the relative density of the prepared MG-based composites exceeded 96.5%. Utilizing such strategy, continuous and precise regulation (0.065 ppm/K corresponds to one percent of the volume) of the CTE over a broad range (9.6 ppm/K to 34 ppm/K) is achieved. In addition, composite with NZTE property (average 0.19 ppm/K) over a very wide temperature range (220 K to 480 K) was successfully prepared by adding 60 vol% of beta-LAS. It is worth mentioning that the prepared NZTE composites also exhibit convenient processability and excellent mechanical properties. Our results provide an excellent strategy for precisely tuning the CTE over a broad wide range, which will greatly

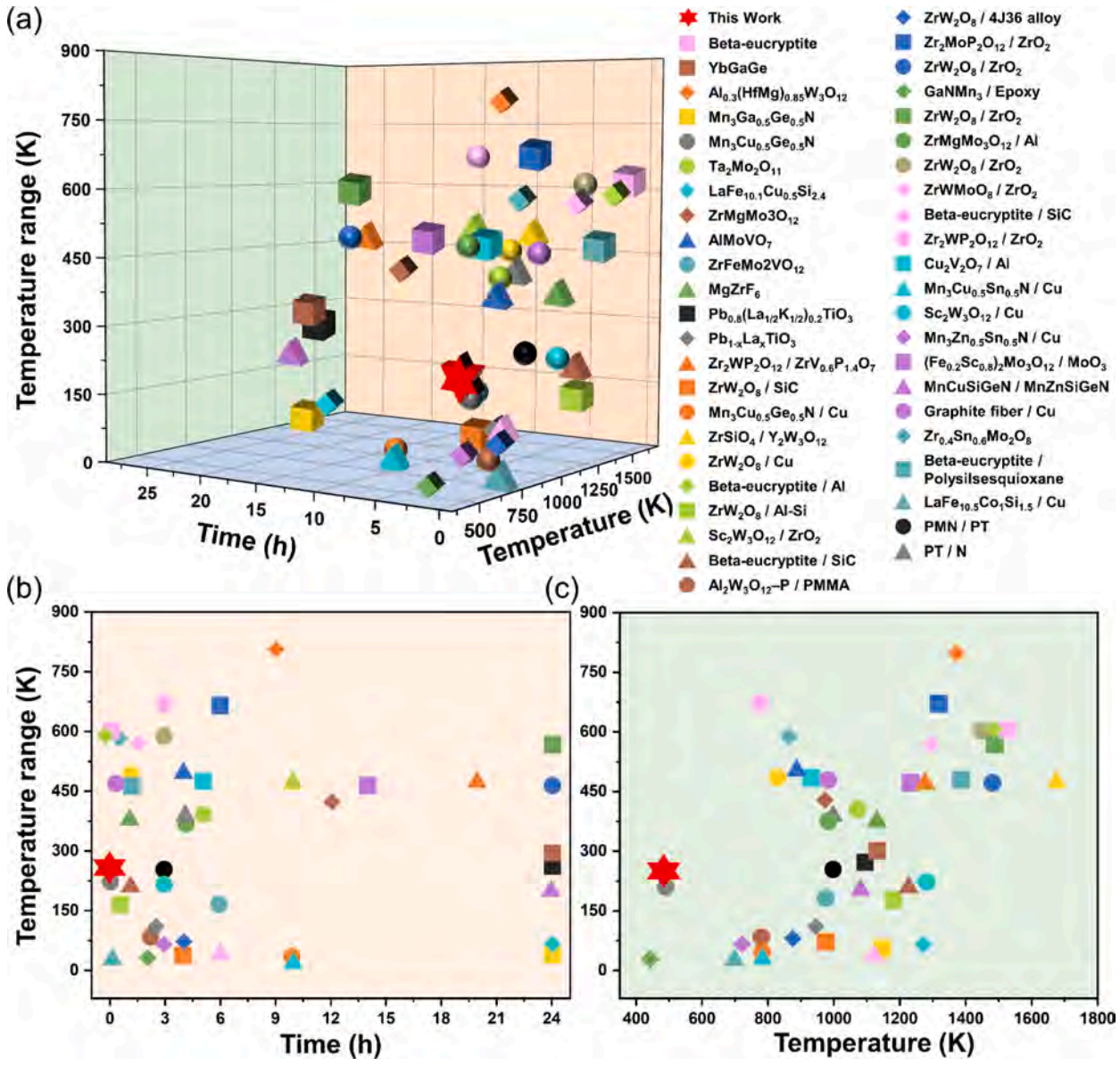

Fig. 5. Summary of processing parameters and temperature range of NZTE materials. (a) Comparison of processing temperature, time and NTZE temperature range of MG-beta-LAS composites with other near-zero expansion materials. (b) Corresponding relationship between processing time and NTZE temperature range. (c) Corresponding relationship between processing temperature and NTZE temperature range.

meet the application in the field of temperature-sensitive functional materials and devices.

Data availability

The data that support the findings of this study are available from the corresponding author upon reasonable request.

CRediT authorship contribution statement

Fei Sun: Methodology, Validation, Formal analysis, Investigation, Data curation, Writing – original draft, Writing – review & editing, Visualization. **Hongji Lin:** Investigation, Methodology, Validation, Project administration. **Jianan Fu:** Methodology, Investigation. **Zhen Li:** Writing – review & editing, Visualization. **Feng Luo:** Investigation, Supervision. **Bei Wang:** Investigation, Supervision. **Wenqing Ruan:** Investigation, Supervision. **Shuai Ren:** Investigation, Supervision. **Zhenxuan Zhang:** Investigation, Supervision. **Xiong Liang:** Supervision. **Jiang Ma:** Investigation, Writing – review & editing, Supervision. **Jun Shen:** Investigation, Visualization.

Declaration of Competing Interest

The authors declare that they have no known competing financial interests or personal relationships that could have appeared to influence the work reported in this paper.

Acknowledgments

The work was supported by the Key Basic and Applied Research Program of Guangdong Province, China (Grant Nr. 2019B030302010), the NSF of China (Grant Nr. 52122105, 51871157, 51971150), the National Key Research and Development Program of China (Grant No. 2018YFA0703605). The authors also thank the assistance on microscope observation received from the Electron Microscope Center of the Shenzhen University.

Supplementary materials

Supplementary material associated with this article can be found, in the online version, at doi:10.1016/j.apmt.2022.101565.

References

[1] J.A. Monroe, D. Gehring, I. Karaman, R. Arroyave, D.W. Brown, B. Clausen, Tailored thermal expansion alloys, Acta Mater. 102 (2016) 333–341, https://doi.org/10.1016/j.actamat.2015.09.012.
[2] N. Yamamoto, E. Gdoutos, R. Toda, V. White, H. Manohara, C. Daraio, Thin films with ultra-low thermal expansion, Adv. Mater. 26 (2014) 3076–3080, https://doi.org/10.1002/adma.201304997.
[3] T.A. Mary, J.S.O. Ecans, T. Vogt, A.W. Sleight, Negative thermal expansion from 0.3 to 1050 Kelvin in ZrW2O8, Science 272 (1996), https://doi.org/10.1126/science.272.5258.90.
[4] R. Roy, D.K. Agrawal, H.A. Mckinstry, Very low thermal expansion coefficient materials, Annu. Rev. Mater. Sci. 19 (1989) 59–81, https://doi.org/10.1146/annurev.ms.19.080189.000423.
[5] M.M. Toropova, C.A. Steeves, Adaptive bimaterial lattices to mitigate thermal expansion mismatch stresses in satellite structures, Acta Astronaut. 113 (2015) 132–141, https://doi.org/10.1016/j.actaastro.2015.03.022.
[6] A. Sleight, Materials science: zero-expansion plan, Nature 425 (2003) 674–676, https://doi.org/10.1038/425674a.
[7] Y. Zhang, B. Chen, D. Guan, M. Xu, R. Ran, M. Ni, W. Zhou, R. O'Hayre, Z. Shao, Thermal-expansion offset for high-performance fuel cell cathodes, Nature 591 (2021) 246–251, https://doi.org/10.1038/s41586-021-03264-1.
[8] E. Boatti, N. Vasios, K. Bertoldi, Origami metamaterials for tunable thermal expansion, Adv. Mater. 29 (2017), https://doi.org/10.1002/adma.201700360.
[9] S. Komura, G.. Lippmann, W. Schmatz, Magnetic cluster structures in an iron–nickel invar alloy, J. Appl. Crystallogr. 7 (1974) 233–236, https://doi.org/10.1107/S0021889874009447.
[10] X. Liang, X. Zhu, X. Li, R. Mo, Y. Liu, K. Wu, J. Ma, High-entropy alloy and amorphous alloy composites fabricated by ultrasonic vibrations, Sci. China Phys. Mech. Astron. 63 (2020) 1–5, https://doi.org/10.1007/s11433-020-1560-4.
[11] J. Fu, J. Yang, K. Wu, H. Lin, W. Wen, W. Ruan, S. Ren, Z. Zhang, X. Liang, J. Ma, Metallic glue for designing composite materials with tailorable properties, Mater. Horiz. (2021) 1690–1699, https://doi.org/10.1039/D1MH00521A.
[12] O. Sigmund, S. Torquato, Composites with extremal thermal expansion coefficients, Appl. Phys. Lett. 69 (1996) 3203–3205, https://doi.org/10.1063/1.117961.
[13] J. Ma, C. Yang, X. Liu, B. Shang, Y. Yang, Fast surface dynamics enabled cold joining of metallic glasses, Sci. Adv. 5 (2019) eaax7256, https://doi.org/10.1126/sciadv.aax7256.
[14] C. Zhou, Y. Zhou, Q. Zhang, Q. Meng, L. Zhang, E. Kobayashi, G. Wu, Near-zero thermal expansion of ZrW2O8/Al–Si composites with three dimensional interpenetrating network structure, Compos. Part B Eng. 211 (2021), 108678, https://doi.org/10.1016/j.compositesb.2021.108678.
[15] C. Zhou, Q. Zhang, X. Tan, S. Deng, K. Shi, C. wang, G. Wu, Fully-dense Mn3Zn0.7Ge0.3N/Al composites with zero thermal expansion behavior around room temperature, Materialia 6 (2019), 100289, https://doi.org/10.1016/j.mtla.2019.100289.
[16] O.N. Kryukova, A.G. Knyazeva, V.M. Pogrebenkov, K.S. Kostikov, I. Sevostianov, Effective thermal expansion coefficient of a sintered glass–eucryptite composite, J. Mater. Sci. 52 (2017) 11314–11325, https://doi.org/10.1007/s10853-017-1298-9.
[17] C. Zhou, Q. Zhang, S. Liu, T. Zhou, J.R. Jokisaari, G. Wu, Microstructure and thermal expansion analysis of porous ZrW2O8/Al composite, J. Alloy. Compd. 670 (2016) 182–187, https://doi.org/10.1016/j.jallcom.2016.02.021.
[18] Z. Peng, Y.Z. Sun, L.M. Peng, Hydrothermal synthesis of ZrW2O8 nanorods and its application in ZrW2O8/Cu composites with controllable thermal expansion coefficients, Mater. Des. 54 (2014) 989–994, https://doi.org/10.1016/j.matdes.2013.09.012.
[19] E. Della Gaspera, R. Tucker, K. Star, E.H. Lan, Y.S. Ju, B. Dunn, Copper-based conductive composites with tailored thermal expansion, ACS Appl. Mater. Interfaces 5 (2013) 10966–10974, https://doi.org/10.1021/am403227c.
[20] Y. Wu, M. Wang, Z. Chen, N. Ma, H. Wang, The effect of phase transformation on the thermal expansion property in Al/ZrW_2O_8 composites, J. Mater. Sci. 48 (2012) 2928–2933, https://doi.org/10.1007/s10853-012-6933-x.
[21] H. Holzer, D.C. Dunand, Phase transformation and thermal expansion of Cu/ZrW_2O_8 metal matrix composites, J. Mater. Res. 14 (1998) 780–789, https://doi.org/10.1557/jmr.1999.0104.
[22] Z.W. Xue, L.D. Wang, Z. Liu, W.D. Fei, Effect of interfacial state on thermal expansion behaviors of β-LiAlSiO4 particulate-reinforced Cu composites, Scr. Mater. 62 (2010) 867–870, https://doi.org/10.1016/j.scriptamat.2010.02.022.
[23] G. Wu, C. Zhou, Q. Zhang, R. Pei, Decomposition of ZrW2O8 in Al matrix and the influence of heat treatment on ZrW_2O_8 /Al–Si thermal expansion, Scr. Mater. 96 (2015) 29–32, https://doi.org/10.1016/j.scriptamat.2014.10.014.
[24] J. Tani, M. Takahashi, H. Kido, Fabrication and thermal expansion properties of ZrW_2O_8/$Zr_2WP_2O_{12}$ composites, J. Eur. Ceram. Soc. 30 (2010) 1483–1488, https://doi.org/10.1016/j.jeurceramsoc.2009.11.010.
[25] A.L. Greer, Metallic glasses, Science 31 (1995) 1947–1953, https://doi.org/10.1126/science.267.5206.1947.
[26] N. Li, Y. Chen, M.Q. Jiang, D.J. Li, J.J. He, Y. Wu, L. Liu, A thermoplastic forming map of a Zr-based bulk metallic glass, Acta Mater. 61 (2013) 1921–1931, https://doi.org/10.1016/j.actamat.2012.12.013.
[27] G. Kumar, H.X. Tang, J. Schroers, Nanomoulding with amorphous metals, Nature 457 (2009) 868–872, https://doi.org/10.1038/nature07718.
[28] J. Schroers, Q. Pham, A. Peker, N. Paton, R.V. Curtis, Blow molding of bulk metallic glass, Scr. Mater. 57 (2007) 341–344, https://doi.org/10.1016/j.scriptamat.2007.04.033.
[29] G. Duan, A. Wiest, M.L. Lind, J. Li, W.-K. Rhim, W.L. Johnson, Bulk metallic glass with benchmark thermoplastic processability, Adv. Mater. (2007) 4272–4275, https://doi.org/10.1002/adma.200700969.
[30] J. Schroers, Highly processable bulk metallic glass-forming alloys in the Pt–Co–Ni–Cu–P system, Appl. Phys. Lett. 84 (2004) 3666–3668, https://doi.org/10.1063/1.1738945.
[31] H. Li, Z. Li, J. Yang, H.B. Ke, B. Sun, C.C. Yuan, J. Ma, J. Shen, W.H. Wang, Interface design enabled manufacture of giant metallic glass, Sci. China Mater. 64 (2021) 964–972, https://doi.org/10.1007/s40843-020-1561-x.
[32] F. Sun, B. Wang, F. Luo, Y.Q. Yan, H.B. Ke, J. Ma, J. Shen, W.H. Wang, Shear punching of bulk metallic glasses under low stress, Mater. Des. 190 (2020), 108595, https://doi.org/10.1016/j.matdes.2020.108595.
[33] F. Luo, F. Sun, K. Li, F. Gong, X. Liang, X. Wu, J. Ma, Ultrasonic assisted micro-shear punching of amorphous alloy, Mater. Res. Lett. 6 (2018) 545–551, https://doi.org/10.1080/21663831.2018.1500399.
[34] E. ASTM, Standard Test Methods of Compression Testing of Metallic Materials at Room Temperature, ASTM International, PA, 2000, pp. 98–105.
[35] V. Drebushchak, Thermal expansion of solids: review on theories, J. Therm. Anal. Calorim. 142 (2020) 1097–1113, https://doi.org/10.1007/s10973-020-09370-y.
[36] P.S. Turner, Thermal-expansion stresses in reinforced plastics, J. Res. Natl. Bur. Stand. 37 (1946) 239–250.